2023-08-19

Role of atmospheric indices in describing shoreline variability along the Atlantic coast of Europe

Masselink, Gerd

Role of atmospheric indices in describing shoreline variability along the Atlantic coast of Europe

Gerd Masselink[1], Bruno Castelle[2], Aikaterini Konstantinou[1] and Tim Scott[1]*

[1]Coastal Processes Research Group, University of Plymouth, Plymouth, PL4 8AA, UK
[2]University Bordeaux, CNRS, Bordeaux INP, EPOC UMR 5805, Pessac, 33600, France.

[*]Corresponding author: gerd.masselink@plymouth.ac.uk
Contributing authors: bruno.castelle@u-bordeaux.fr, a.konstantinou@plymouth.ac.uk, timothy.scott@plymouth.ac.uk

Submitted to Geophysical Research Letters

Abstract (150 words)

Beaches are highly variable environments and respond to changes in wave forcing, themselves modulated by climate variability. Here, we analyse three high-quality beach profile datasets to robustly investigate, for the first time, the link between shoreline change, wave forcing and climate variability along the Atlantic coast of Europe. Winter wave conditions are strongly associated with North Atlantic Oscillation (NAO) and Western Europe Pressure Anomaly (WEPA), with WEPA explaining 50–80% of the winter wave power variability. Shoreline variability during winter is also strongly linked to NAO and WEPA, with WEPA explaining 25% of the winter shoreline variability. Winter wave conditions and associated shoreline variability are both unrelated to El Nino Southern Oscillation (ENSO). In addition to the atmospherically-forced beach morphological response, shoreline change also depends strongly on the antecedent conditions as evidenced by significant correlations between summer/winter shoreline response and the shoreline position at the start of each season.

Keywords

Beaches, Atmospheric indices, Shoreline variability, Storms

Key messages

- Three beach profile datasets are used to investigate link between shoreline change, wave forcing and climate variability along the Atlantic coast of Europe for the first time.
- Winter wave conditions and shoreline change are correlated with atmospheric indices NAO and WEPA, but uncorrelated to ENSO
- Antecedent beach morphology is an important factor in determining summer and winter shoreline response

Plain language abstract (150 words)

Beaches change as a result of changes in the wave conditions, and the weather and climate controls wave conditions. We surveyed two beaches in SW England and one beach in SW France every month for more than 15 years and analysed these data to look, for the first time, at the connections between beach change, waves and climate along the Atlantic coast of Europe. Atmospheric indices are numbers that tell us about large-scale weather, and the North Atlantic Oscillation (NAO) and the

Western Europe Pressure Anomaly (WEPA) are powerful indices that describe the weather in the north-east Atlantic. We found that especially WEPA is strongly correlated with winter waves and beach change during the winter months for all three study sites. We also found that beach change over the summer and winter season depends very much on whether the beach is relatively healthy or depleted of sediment.

Introduction

Shorelines are temporally highly variable and amongst the different timescales of shoreline change, the interannual and decadal timescales are of particular interest to coastal scientists as they reflect the integrated system response to the Earth's climate and its natural modes of variability. On these short-to-medium time scales, wave variability is the main driver for shoreline change and beaches respond to individual storms *(Harley et al., 2017)*, storm clusters *(Dissanayake et al., 2015)*, seasonal variation in wave conditions *(Masselink and Pattiaratchi, 2001)* and inter-annual to decadal changes in wave forcing *(Castelle et al., 2018)*. Shorelines are also expected to change over long-term (> 25 years) time scales, for example due to sea-level rise, but, even when using decadal data sets, it has been challenging to identify and isolate the modest and longer-term shoreline trends from the much more dynamic and short-to-medium term changes imposed by wave climate variability *(Ghanavati et al., 2023)*. Both wave-driven cross-shore and longshore sediment transport processes are responsible for changes in beach morphology and shoreline position, with cross-shore processes generally dominating seasonal and annual coastal change, whereas longshore processes tend to dominate the coastal response over decadal times *(Vitousek et al., 2017)*.

Temporal changes in wave forcing are controlled by large-scale weather patterns and their variability. Across the Pacific Ocean basin, the El Niño-Southern Oscillation (ENSO) is the dominant mode of interannual climate variability and is closely associated with wave conditions *(Boucharel et al., 2021)*. In the Indian Ocean, seasonal extreme wave heights are associated with different phase combinations of ENSO and the Indian Ocean Dipole IOD *(Kumar et al., 2019)*. In the north Atlantic, the North Atlantic Oscillation (NAO) is the dominant mode of atmospheric variability and is strongly associated with wave conditions, whereby the positive phase of NAO is associated with increased winter wave conditions across the northeast Atlantic *(Dodet et al., 2010)*, whereas the negative phase of NAO is associated with energetic wave conditions along the south coast of Spain *(Plomaritis et al., 2015)*. These dominant atmospheric circulation patterns can be quantified using indices, generally based on a measure of spatial variability in sea surface temperature or atmospheric pressure over a region of interest, and can be correlated with wave parameters to investigate associations.

For the northeast Atlantic, *Castelle et al. (2017b)* recently introduced a new atmospheric index, the Western Europe Pressure Anomaly (WEPA), based on the sea level pressure (SLP) gradient between the Valentia (Ireland) and Santa Cruz de Tenerife (Canary Islands). The WEPA positive phase reflects an intensified and southward-shifted SLP difference between the Icelandic low and the Azores high, driving severe storms that funnel high-energy waves toward western Europe southward of 52°N. The WEPA index was found to show a very strong correlation with winter wave conditions for the entire Atlantic European seaboard, from Ireland (52ºN) to Spain (42ºN), significantly outperforming NAO as a winter wave height predictor. Within the UK and Ireland, *Scott et al. (2021)* used wave model data from 63 locations and found that winter-averaged expressions of six leading atmospheric indices (including NAO and WEPA) were strongly correlated with both total and directional winter wave power. Notably, the predictive power of the climate indices displayed a strong geographical dependency, with NAO, and especially WEPA, being the most successful predictor for Atlantic storm waves. More regionally, *Wiggins et al. (2020)* investigated the characteristics of the strong bidirectional wave climate along the SE of England. They showed south-westerly wave power was well correlated to WEPA>0, whilst easterly wave power was well correlated with NAO<0.

Since wave height variability is strongly linked to coastal dynamics, it can therefore be hypothesized that atmospheric indices are also linked to coastal change. *Almar et al. (2023)* used this hypothesis on a global scale by developing a conceptual global model based on satellite-derived shoreline (SDS) positions from 1993 to 2019 and a variety of reanalysis products. They argue that global interannual

shoreline changes are largely driven by different ENSO regimes and their complex inter-basin teleconnections, although there is some discussion with regards of the validity of these findings *(Warrick, 2024)*. Nevertheless, extreme coastal erosion along the west coast of the US is unequivocally associated with strong El Niño events *(Barnard et al., 2011; Barnard et al., 2017; Young et al., 2018)*. Recently, *Vos et al. (2023)* used 38 years of Landsat imagery to map shoreline variability around the Pacific Rim and identified coherent, albeit regionally varying, patterns of beach erosion and accretion controlled by ENSO.

Similar efforts have been made to find associations between atmopsheric indices and coastal change for the Atlantic coast of Europe. *Masselink et al. (2014)* suggested, based on analysis of a decade of video monitoring data from a sandy beach in SW England, that beach state and bar morphology is related to NAO. *Wiggins et al. (2020)* analyzed a decade of beach monitoring data from gravel beaches in SW England and found that beach rotation was related to WEPA for some beaches. Additionally, the 2013/14 winter, which was the most energetic winter on record in terms of wave conditions and caused unprecedented beach erosion along the entire Atlantic coast of Europe *(Masselink et al., 2016a)*, was characterized by the highest winter WEPA value since 1948. Finally, *Castelle et al. (2022)* investigated the 1984–2020 time- and space-evolution of 269 km of high-energy meso-macrotidal sandy coast in SW France using SDS data and found that the interannual shoreline variability was strongly correlated with the winter WEPA, outscoring other conventional teleconnection pattern indices (e.g., NAO). The attraction of identifying causal links between atmospheric indices and shoreline change is that it may facilitate modelling future shoreline dynamics without the need for wave modelling *(Robinet et al., 2016)*, for example, to obtain season-ahead forecast of coastal change *(Scott et al., 2021)*.

This paper builds on previous work along the Atlantic coast of Europe and uses a 17-year dataset of monthly survey data collected at two beaches in SW England, Perranporth (sand) and Slapton Sands (gravel), and a 20-year high-frequency dataset of from sandy beach in SW France (Truc Vert) to investigate the link between atmospheric indices, wave conditions and shoreline change. This is a first attempt at a wider scale (NW Atlantic coast) assessment of the links between climate patterns and shoreline change and this work represents a crucial step needed to gain confidence before investigating climate-shoreline links in larger-scale SDS-based studies.

Results

Perranporth

Winter wave power ΣP at Perranporth (Fig. **1a**) is positively correlated with winter NAO (Fig. **1c**; r=0.63, p=0.01) and WEPA (Fig. **1d**; r=0.71, p=0.00), indicating that positive phases of both atmospheric indices are associated with enhanced storminess. No significant correlation was found with ENSO (r=-0.23; p=0.36). The monthly time series of shoreline position x at Perranporth shows a strong seasonal variation with an amplitude of 20–30 m (Fig. **1b**). No long-term trend is apparent, but a dominant feature of the time series is a shoreline retreat of c. 60 m during the 2013/2014 winter. All summers are characterized by shoreline progradation (Δx>0) and all winters resulted in shoreline retreat (Δx<0). The seasonality in shoreline change is further demonstrated by the auto-correlation function of the monthly survey data, which shows a distinct secondary peak at 12 months (Fig. **1e**). Beach morphological change at Perranporth is forced by variations in the wave conditions, but is also influenced by the antecedent morphology. A strong correlation between the seasonal shoreline change Δx and the seasonally averaged wave height H_s is apparent (Fig. **1f**; r=-0.83, p=0.00)), with H_s=1.5 m broadly separating shoreline advance and retreat. Seasonal shoreline response is also affected by the shoreline position at the start of the season: winter erosion (Δx<0) is encouraged when the beach is relatively wide at the start of the winter (Fig. **1g**; r=-0.54, p=0.03), while summer accretion is promoted by a relatively depleted beach at the start of summer (Fig. **1h**; r=-0.42, p=0.10).

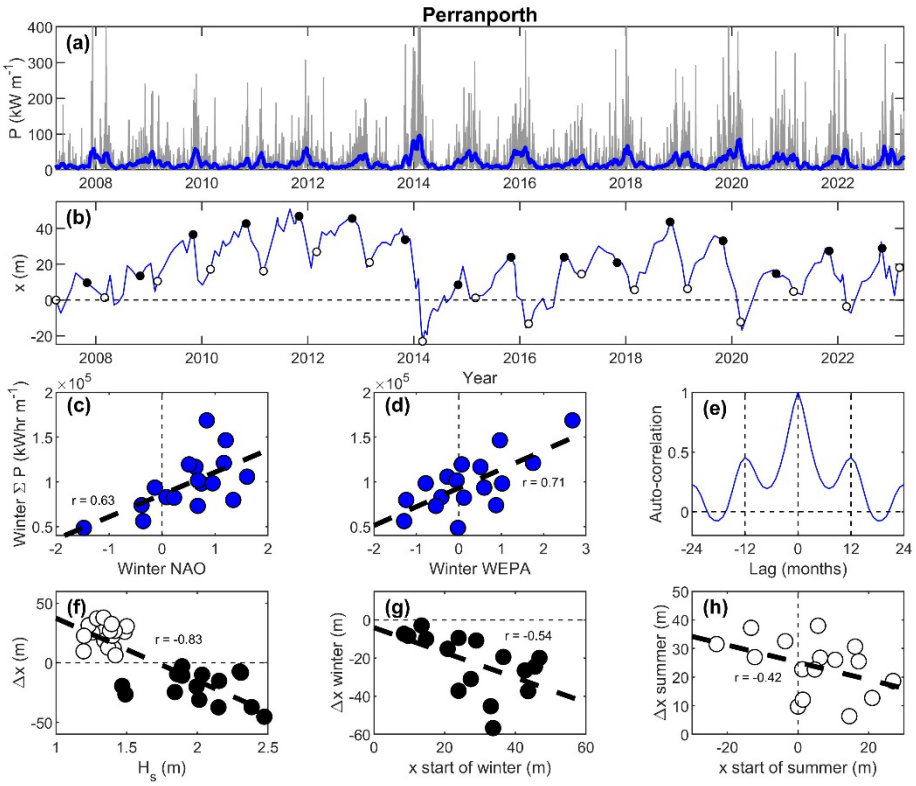

Fig. 1. Wave conditions and shoreline response for Perranporth: (a) time series of wave power P (grey line) and 30-day moving average of the wave power (blue line); (b) time series of monthly shoreline position x (0 m ODN) relative to start of the survey period with start of winter (1 December) and summer (1 April) marked by black and white circles, respectively; (c,d) scatter plot of winter wave power ΣP versus winter NAO and WEPA; (e) auto-correlation function of the monthly survey data; (f) shoreline change Δx versus season-averaged significant wave height H_s with black and white circles representing winter and summer, respectively; (g) Δx over winter season versus x at the start of winter; and (h) Δx over summer season versus x at the start of summer. Dashed lines in (c), (e), (f) and (g) represent lines of best fit with Pearson r indicated in the plots.

Slapton Sands

The wave climate at Slapton Sands is bi-directional with 70% of the winter wave power generated by southerly swell waves from the Atlantic and 30% by easterly wind waves generated across the Channel (Fig. **2a**). Southerly wave power from the Atlantic ΣP_{south} is positively correlated with winter WEPA (Fig. **2d**; r=0.89, p=0.00), whereas easterly wave power ΣP_{east}, is correlated with winter NAO (Fig. **2c**; r=0.53, p=0.03) indicating that large ΣP_{east} values are associated with negative NAO). No significant correlations were found with ENSO (with ΣP_{south}: r=-0.1, p=0.70; with ΣP_{east}: r=-0.34, p=0.20). Shoreline changes at Slapton Sands are characterized by an antiphase relationship between the south and north end of the beach (P01 and P18, respectively) (Fig. **2b**), representing a rotational response. Over the whole survey period, the southern profile shows a shoreline retreat of 15 m, whereas the northern profile displays a shoreline advance of 30 m. Seasonal shoreline variation is not obvious, but the largest shoreline changes are generally associated with winter waves. Both winter waves and summer waves can result in a shoreline advance, as well as retreat. The lack of seasonality is further demonstrated by the absence of a 12-month peak in the auto-correlation function of the monthly survey data for both transects (Fig. **2e**).

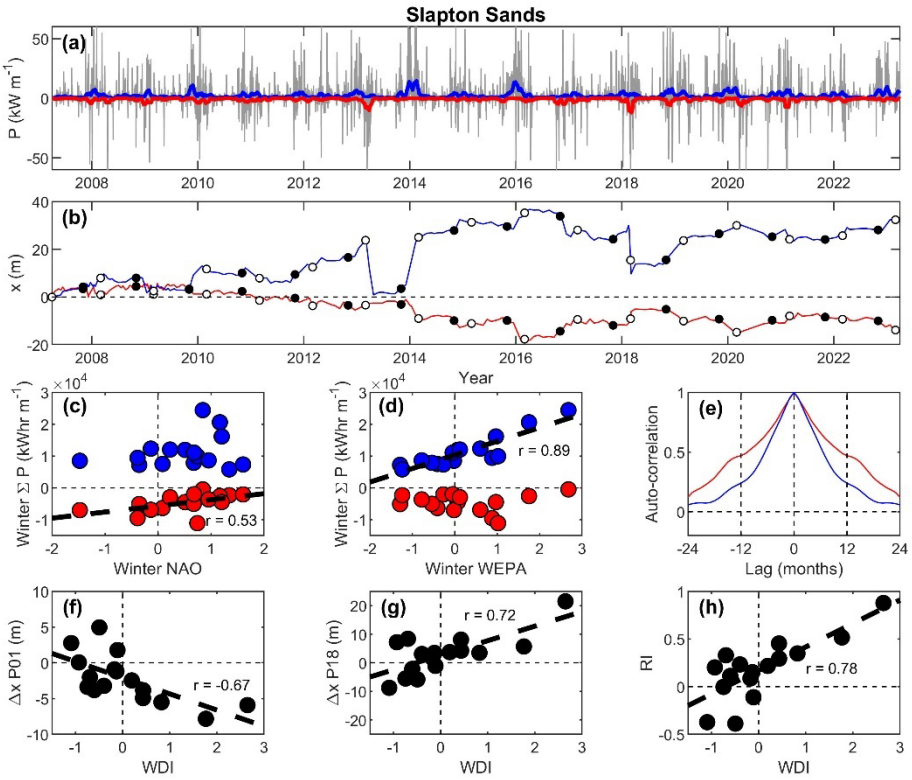

Fig. 2. Wave conditions and shoreline response for Slapton Sands: (a) time series of wave power P (grey line) and 30-day moving average of the southerly (> 135°; blue line) and easterly (< 135°; red line) wave power; (b) time series of monthly shoreline position x (0 m ODN) for P01 (red) and P18 (blue) relative to start of the survey period with start of winter (1 December) and summer (1 April) marked by black and white circles, respectively; (c,d) scatter plot of winter wave power from the south ΣP_{south} (blue) and the east ΣP_{east} (red) versus winter NAO and WEPA; (e) auto-correlation function of the monthly survey data for P01 (red line) and P18 (blue line); (h,i) winter shoreline change Δx at P01 and P18 versus winter Directional Power index *WDI*; and (j) Rotation Index *RI* versus *WDI*. Positive and negative values for *WDI* represent above-average contribution of southerly and easterly wave power, respectively, and positive and negative values for *RI* represent clockwise and anti-clockwise beach rotation, respectively. Dashed lines in (c), (d), (f), (g) and (h) represent lines of best fit with Pearson r indicated in the plots.

The more complex beach volume changes at Slapton Sands, involving longshore redistribution of sediment, require consideration of the directional wave energy fluxes for the opposing ends of the beach. Large values of the seasonally integrated southerly wave power ΣP_{south} are associated with shoreline retreat ($\Delta x<0$) and advance ($\Delta x>0$) for P01 and P18, respectively (Fig. **S8a,c**), and a clockwise beach rotation. The beach response to the seasonally integrated easterly wave power ΣP_{east} is not obvious (Fig. **S8b,d**). A better way to parameterize the bi-directional wave conditions at Slapton Sands is through the Wave Directional Index *WDI* (see **Methods** section in Supp. Mat.), which quantifies the seasonal balance between the two directional wave components compared to the long-term average balance. *WDI* is significantly correlated with Δx at P01 (Fig. **2f**; r=-0.67, p=0.00) and at P18 (Fig. **2g**; r=0.72, p=0.00). By combining the shoreline responses at the opposing ends of Slapton Sands in the Rotation Index *RI* (see **Methods** section in Supp. Mat.) and relating this to *WDI* provides an even better explanation of the rotational beach response (Fig. **2h**; r=-0.78, p=0.00): for *WDI*>0, southerly waves are more common than average and/or easterly waves are less common than average, and the beach at P01 and P18 retreats and advances, respectively, and the reverse is true for *WDI*<0. So, clockwise (*RI*>0) and anti-clockwise (*RI*<0) rotation are associated with *WDI*>0 and *WDI*<0, respectively.

Truc Vert

The relationship between atmospheric indices, wave forcing and shoreline dynamics at Truc Vert is very similar to that at Perranporth, despite the more energetic waves and smaller tides. Winter wave power ΣP is positively correlated with winter NAO (Fig. **3c**; r=0.43, p=0.05) and WEPA (Fig. **3d**;

r=0.88, p=0.00), and no significant correlation was found with ENSO (r=-0.09, p=0.71). The shoreline at Truc Vert shows no long-term trend, but has a strong seasonal variation with an amplitude of 10–20 m (Fig. **3b**) and the auto-correlation function of the monthly survey data shows a distinct secondary peak at 12 months (Fig. **3e**). The 2013/2014 winter caused the largest shoreline retreat, and it is further noted that five of the 20 winters were characterized by shoreline progradation and that shoreline retreat occurred over three of the 19 summers. In common with Perranporth, beach morphological change on Truc Vert is also influenced by antecedent morphology. A strong correlation between the seasonal shoreline change Δx and the seasonally averaged wave height H_s is apparent (Fig. **3f**; r=-0.80, p=0.00), but the H_s value separating shoreline advance and retreat is not very distinct. Winter erosion (Δx<0) is encouraged when the beach is relatively wide at the start of the winter (Fig. **3g**; r=-0.52, p=0.02), while summer accretion is promoted by a relatively depleted beach at the start of summer (Fig. **3h**; r=-0.49, p=0.04). The shoreline response on Truc Vert is more complex than at Perranporth and this is likely related to the more energetic conditions at the former site over the summer period (April–November).

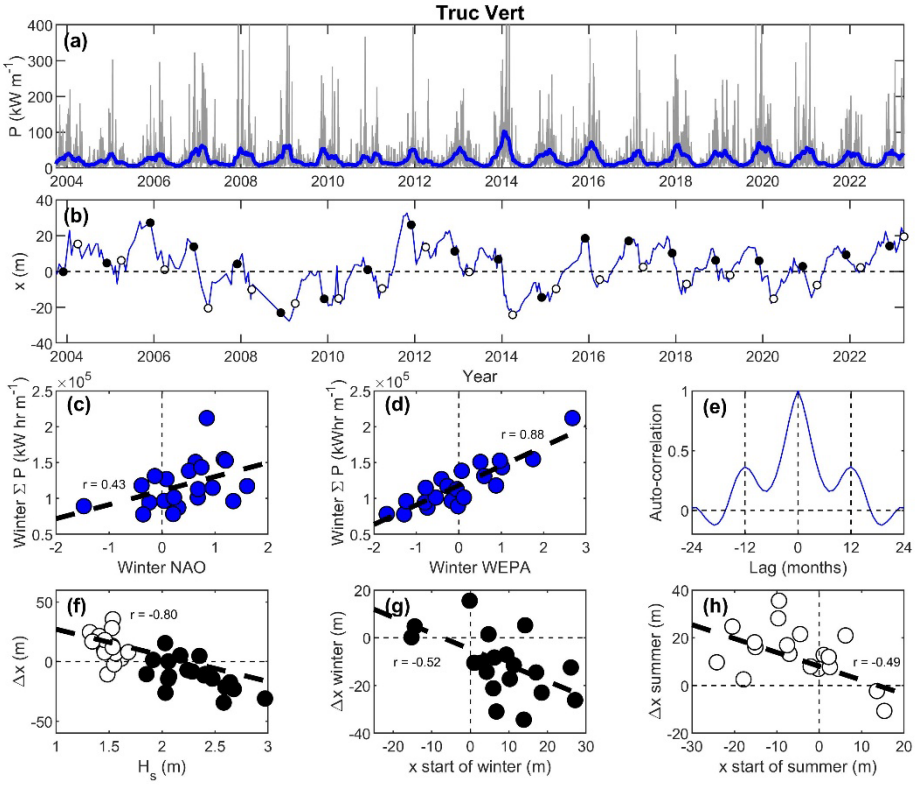

Fig. **3**. Wave conditions and shoreline response for Truc Vert (for caption, cf. Fig. **1**).

Role of atmospheric indices

As the winter-averaged atmospheric indices NAO and WEPA are strongly correlated to the winter wave climate and the shoreline dynamics are strongly related to the wave climate, it seems appropriate to address the relationship between shoreline change Δx and atmospheric indices for the winter season (Fig. **4**). The strength of the correlations between climate indices and wave forcing and shoreline response (Pearson r and associated p-values) are listed in Table **S2**.

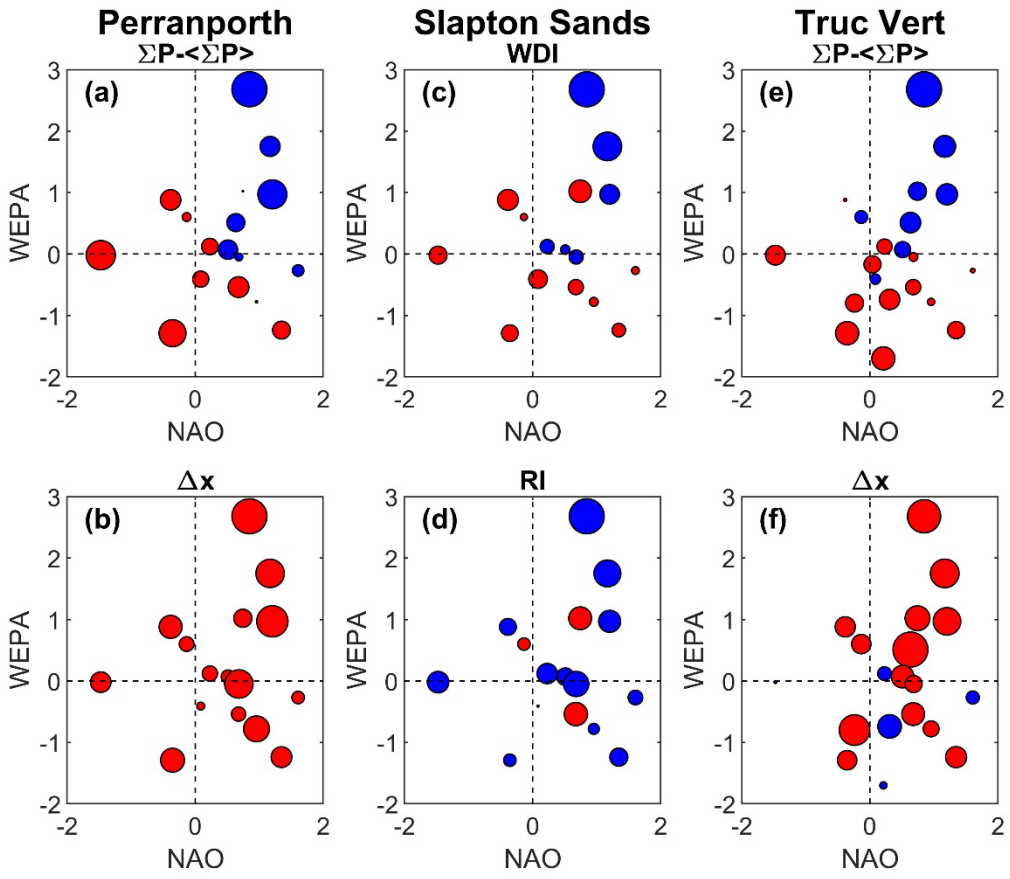

Fig. 4. Wave and morphological response parameters representing the winter season plotted in NAO-WEPA parameter space: (a) winter wave power Σ*P* minus winter-averaged wave power <Σ*P*> for Perranporth; (b) shoreline change Δ*x* for Perranporth; (c) Directional Power index *WDI* for Slapton Sands; (d) Rotation Index *RI* for Slapton Sands; (e) winter wave power Σ*P* minus winter-averaged wave power <Σ*P*> for Truc Vert; and (f) shoreline change Δ*x* for Truc Vert. The size of the symbols is scaled by the absolute value of the plotted parameters, and red and blue symbols represent negative and positive values, respectively.

The winter wave forcing conditions (Σ*P*-<Σ*P*> for Perranporth and Truc Vert, and *WDI* for Slapton Sands) are plotted in a NAO-WEPA parameter space in Fig. **4a,e,c**, respectively (no significant correlations were found with ENSO). The NAO+/WEPA+ quadrant is associated with the most energetic winter wave conditions at Perranporth and Truc Vert, and the largest positive *WDI* values for Slapton Sands. Both results are attributed to more energetic and/or frequent Atlantic storms under such climatic conditions *(Castelle et al., 2017b)*. The other NAO/WEPA quadrants are characterized by more benign and below-average winter wave conditions for Perranporth and Truc Vert, and smaller positive or even negative *WDI* values for Slapton Sands. As *WDI* represents the balance between southerly and easterly wave power, negative *WDI* values could be due to less energetic Atlantic wave conditions and/or more frequent easterly storm wave activity.

The winter beach response (Δ*x* for Perranporth and Truc Vert, and *RI* for Slapton Sands) are also plotted in the NAO-WEPA parameter space (again, no significant correlations were found with ENSO). The most extensive winter shoreline retreat on Perranporth and Truc Vert is associated with the NAO+/WEPA+ quadrant (Fig. **4b,f**) and, of the two atmospheric indices, WEPA shows stronger correlations with Δ*x* than NAO (Table **S2**). At Perranporth, all winters result in shoreline retreat (Fig. **4b**), but the calmest winters at Truc Vert are associated with shoreline advance (blue symbols in Fig. **4f**). For Slapton Sands, the NAO+/WEPA+ quadrant is characterized by the most pronounced clockwise rotation, quantified by *RI*, and the two winters with the largest *RI* values (2013/14 and 2015/16), plot at the top of the NAO+/WEPA+ quadrant (Fig. **3d**). Of the two climate indices, WEPA shows stronger correlation with RI than NAO (Table **S2**).

Discussion and conclusions

The findings of this study, based on three European Atlantic coast observational data sets consisting of (bi-)monthly observational beach profile data collected over >15 years, confirm and expand previous studies on these three beaches *(Castelle et al., 2020; McCarroll et al., 2023)*. Winter wave conditions for all three sites are strongly associated with Atlantic climate indices NAO and WEPA, and are unrelated to ENSO. Perranporth and Truc Vert, which are representative of exposed Atlantic sandy beaches, experience a unidirectional and strongly seasonal wave climate, which drives a dominantly cross-shore and seasonal beach signal. Slapton Sands, which is a representative gravel beach on the south coast of England, experiences a bidirectional wave climate, which drives a dominantly rotational beach response caused by a longshore redistribution of sediment. The morphodynamics on all three beaches are strongly linked to Atlantic climate indices NAO and WEPA, and unrelated to ENSO. In addition to the strongly forced response, as testified by the link between beach change and wave conditions and climate indices, beach response on the exposed beaches (Perranporth and Truc Vert) also depends strongly on the beach state/volume at the start of each season.

The strongest statistically significant (at $p<0.05$) correlations are found between WEPA and winter shoreline change; however, winter WEPA only explains c. 25% of the shoreline variability. There are other factors that are also important in driving shoreline change over the winter period. Firstly, pronounced shoreline response is not necessarily the result of sustained storm wave activity related to an exceptional atmospheric condition parameterized by an extreme value for a climate index (e.g., the 2013/14 winter), and can be the result of a single event in an otherwise unremarkable winter. For example, the pronounced anti-clockwise rotation that occurred in the 2018/2019 winter on Slapton Sands (Fig. **2**) was the result of a single easterly storm *(McCarroll et al., 2019)* that occurred in a winter characterized by a positive NAO of 0.74. Secondly, the shoreline dynamics on the exposed and cross-shore dominated beaches of Perranporth and Truc Vert showed relatively muted storm responses on beaches depleted due to previous energetic conditions, strongly suggesting the importance of antecedent conditions and an equilibrium-type beach response *(Yates et al., 2009; Splinter et al., 2014; Davidson, 2021)*. The shoreline response of Slapton Sands appears also to be associated with disequilibrium, but operating over a decadal time scale. Over the 2004–2023 survey period, the shoreline at Slapton Sands exhibited a considerable clock-wise rotation and this has been suggested to be related to a multi-decadal trend in the balance between southerly and easterly wave power *(Wiggins et al., 2017)*. Finally, the role of water levels during storm conditions should be considered as storm impacts are maximized if peak wave conditions coincide with extreme water levels *(Masselink et al., 2016b; Young et al., 2018)*. As the Atlantic coast of Europe is not surge-dominated coast, coincidence of peak storm and extreme water level is due to chance *(Haigh et al., 2016)*, and not related to atmospheric indices.

In this study, the position of the intertidal shoreline (0 m ODN for Perranporth and Slapton Sands and 1.4 m amsl for Truc Vert) was selected as the key Coastal State Indicator (CSI) for characterizing beach morphological response. It was found to be highly correlated with the intertidal beach volume (Fig. **S4**) and a similar analysis to that presented in this paper for the SW England beaches using beach volume as the key morphological change parameter yielded near-identical results *(Masselink et al., 2024)*. The attraction of a shoreline-based CSI is obvious as it can be derived through remote sensing (aerial photography, video, satellites). Nevertheless, changes in the intertidal shoreline position are not necessarily representative of changes in the nearshore sediment budget if the subtidal region is considered as well *(Harley et al., 2022)*. In addition, different shoreline contours respond at different dominant time scales *(Montaño et al., 2021)*, for example, compared to the MSL contour, the dune foot responds in a less seasonal and more multi-annual fashion with significant set-back only occurring during a handful of winters *(Castelle et al., 2017a; Flor-Blanco et al., 2021; Masselink et al., 2022; Burvingt and Castelle, 2023)*.

Winter values for climate indices (December–March) are generally used because they tend to have the strongest relation to wave climate and it is the climate hazards during winter (e.g., dune erosion, coastal flooding, overtopping) that are usually of most interest. So, here we demonstrate that shoreline response during winter is significantly correlated to winter WEPA, and, for example, *Jalón-Rojas and Castelle (2021)* show that precipitation and river flows over the winter period across most of Europe

are also positively correlated with winter WEPA. From a coastal management point of view, it is of interest to determine the longevity of the winter storm impacts; therefore, the annual shoreline response (from December to December) was correlated with winter WEPA (from December to March) for Perranporth and Truc Vert. Compared to correlating winter WEPA with the winter shoreline response, Pearson *r* dropped from -0.54 (p=0.03) to -0.40 (p=0.14) for Perranporth, and from -0.52 (p=0.02) to -0.46 (p=0.06) for Truc Vert. The reduction in explanatory power of WEPA is due to the significant beach recovery that takes place over subsequent summers *(Burvingt et al., 2018; Dodet et al., 2019; Konstantinou et al., 2021)*. Shoreline advance during summer is particularly pronounced after an extreme winter (Fig. **1h** and **3h**) and it is perhaps not surprising that winter WEPA is not correlated to the shoreline response when 1-year periods are considered.

Global studies of shoreline change based on satellite-derived shorelines (SDS) are becoming increasing common *(Luijendijk et al., 2018; Mentaschi et al., 2018; Vousdoukas et al., 2020; Almar et al., 2023; Ghanavati et al., 2023)*; however, concerns have been raised regarding satellite-derived global applications *(Cooper et al., 2020; Zăinescu et al., 2023; Warrick, 2024)*. To explore links between shoreline response and modes of climate variability, robust methodologies for deriving shorelines involving wave and/or tide corrections *(Castelle et al., 2021; Vos et al., 2023)* or time- and spatial-averaging techniques *(Castelle et al., 2022; Warrick et al., 2023)* must be applied. However, the typical time- and space-averaging windows and type of water-level correction are essentially site-specific *(Konstantinou et al., 2023)*, which challenges such global application. Based on SDS, *Almar et al. (2023)* recently claimed that interannual shoreline changes at the global scale are largely driven by different ENSO regimes and their complex inter-basin teleconnections, including along the Atlantic coast of Europe. Noteworthy, the authors used uncorrected SDS data at 0.5° spaced transects. Critically, our contribution shows that, at three intensely monitored sites, which use conventional survey techniques from which accurate shoreline position can be derived, shoreline change is essentially uncorrelated with ENSO. This is perhaps not surprising, as there is no clear consensus as to whether a robust ENSO signal can be detected in the north Atlantic and West Europe region *(Toniazzo and Scaife, 2006)*. We advocate that future, regional to global, SDS assessment must use carefully ground-truth validated, high-resolution data accounting for the diversity of coastal settings to provide robust conclusions on the link between climate modes of variability and coastal response.

Acknowledgements

GM and TS were supported by the UK Natural Environment Research Council (Grant NE/M004996/1; BLUE-coast project) and AK was supported by a PhD studentship awarded by CMAR. The University of Plymouth and the Making Space for Sand Project (part of Defra's Innovative Resilience Programme and managed by Cornwall Council) provided additional financial support for the surveys. BC was supported by Agence Nationale de la Recherche (ANR-21-CE01-0015). Truc Vert beach is a coastal monitoring site labelled by the Service National d'Observation (SNO) Dynalit (https://www.dynalit.fr). The Observatoire de la Côte Aquitaine (OCA) and Observatoire Aquitain des Sciences de l'Univers (OASU) provide additional financial support for the surveys. The authors would like to acknowledge all participants that contributed to the collection of the survey data at the three studied beaches.

Methods

Field sites

Perranporth and Slapton Sands are situated on the macrotidal coast of SW England (Fig. **S1** and **S2a,b**). The coastline is largely embayed with more than 150 separate beaches and 21 estuaries and is highly variable in terms of static (shoreline orientation, geology, sediment size and abundance) and dynamic (waves, tides) boundary conditions; therefore, the resulting beach morphology is also very diverse *(Scott et al., 2011)*. Both Perranporth and Slapton Sands have been widely studied over the past 15 years and the reader is referred to *Valiente et al. (2019)* and *Wiggins et al. (2019)*, respectively, for detailed descriptions of the setting and characteristics of both beaches. Here, only a summary is provided. Perranporth is a 3.5-km long and 400-m wide (at low tide) sandy and dissipative beach (gradient ≈ 0.015) with subtidal and intertidal bar morphology and an extensive

dune system (Fig. **S2a**). The mean summer and winter significant wave height H_s at this location is 1.2 and 2.2 m, respectively, and maximum H_s during winter storms can attain 8 m. Waves along the north coast of SW England are almost exclusively from the west and the mean wave direction is 280º. Slapton Sands is a 4-km long and 100-m (at low tide) gravel and reflective beach (gradient ≈ 0.1) with a maximum elevation of 6 m above MSL and is backed by a fresh water lagoon (Fig. **2b**). Here, the mean summer and winter H_s is 0.5 and 0.9 m, respectively, and maximum H_s during winter storms can attain 5 m. Waves along the south coast of SW England are bi-directional and characterised by swell waves from the south and wind waves from the east. The mean spring tide range at Perranporth and Slapton Sands is 6.3 m and 4.3 m, respectively.

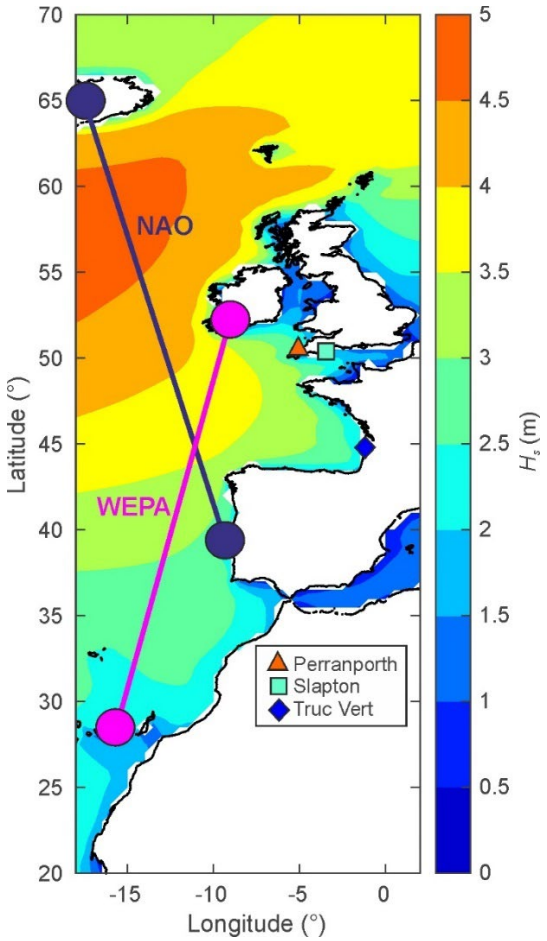

Fig **S1**. Atlantic coast of Europe with winter-mean (2006–2023) significant wave height H_s, locations used for determining NAO and WEPA based on sea-level pressure (SLP), and location of the three studied beaches. In the present paper, WEPA was based on SLP, but NAO was obtained using an PCA-based approach as explained below.

Truc Vert is located along a relative straight sector of the meso-macrotidal coast of SW France (Fig. **S1** and **S2c**). It is an open, intermediate double-barred sandy beach, backed by a high (~20 m) and wide (~200 m) coastal dune system *(Robin et al., 2021)*. The wave climate is similar to that of Perranporth, with mean H_s ranging from 1.1 m in July to 2.4 m in January *(Castelle et al., 2020)*. Waves come predominantly from the W-NW quadrant, with more waves from the W (NW) in winter (summer). The mean spring tide range is approximately 3.7 m.

Time series of wave conditions at all three sites are shown in Figs. **S4**, **S5** and **S6**. All sites are characterised by a pronounced seasonality with energetic winters and relatively calm summers, and Truc Vert represents the most energetic site, while Slapton Sands is the least exposed site (Table **S1**).

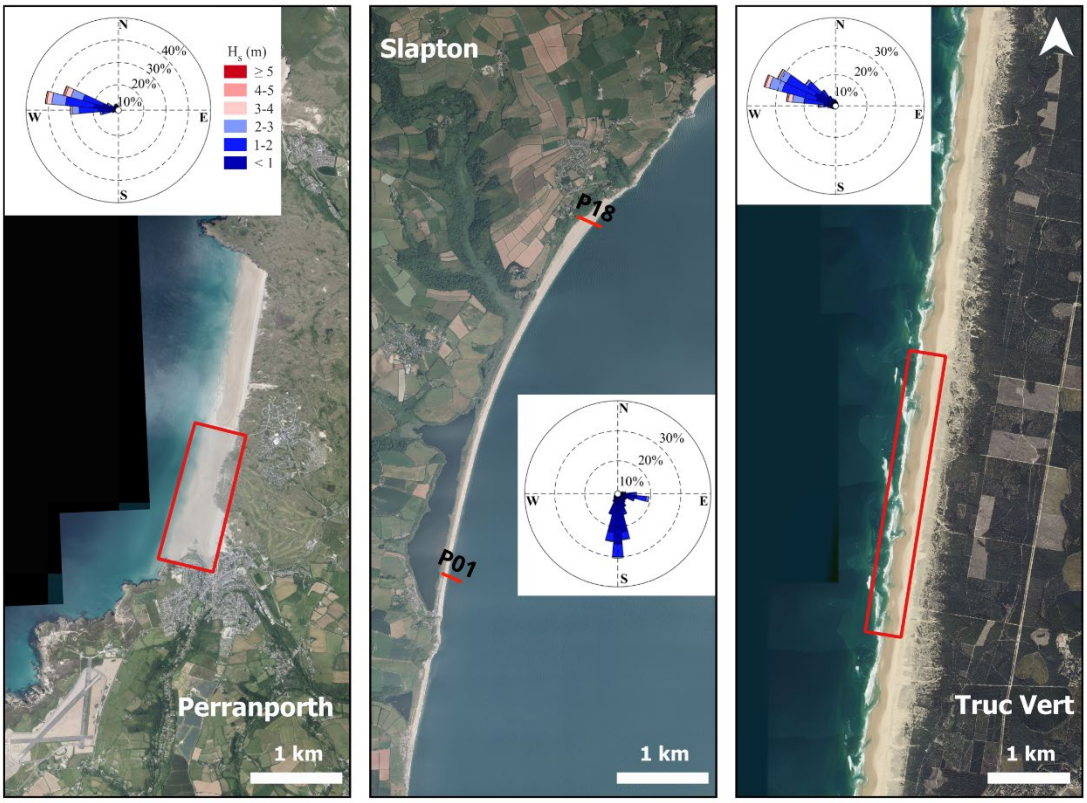

Fig. S2. Aerial photographs of the three studied beaches with wave rose: (a) Perranporth in north Cornwall, UK, with the survey area indicated by red box; (b) Slapton Sands in South Devon, UK, with the southern (P01) and northern (P18) survey transects; and (c) Truc Vert on the Aquitaine coast, France, with the survey area indicated by red box.

Data collection and analysis

Monthly NAO and ENSO (3-month running mean of Southern Oscillation index) were downloaded from https://www.cpc.ncep.noaa.gov/ and the monthly values were used to obtain winter-averaged values, where winter represents the period December–March. These NAO values are not based on sea-level pressure (SLP), but are obtained using the PCA-based approach described in *Barnston and Livezey (1987)*. Monthly WEPA values were directly computed from the SLP records Santa Cruz de Tenerife (Canary Islands) and Valentia (Ireland), obtained from the European Climate Assessment & Dataset (ECA&D; http://www.ecad.eu) and the Irish Meteorological Service (Met Eireann; https://www.met.ie), and used to determine winter-averaged values considering December–March. Time series of the winter values for the climate indices reveal significant variability with alternating positive and negative phases (Fig. **S3a,b,c**). There appears to be a trend towards increasingly positive values in the NAO time series (Fig. **S3a**), which previously has been linked to increased extreme wave conditions over the period (1948–2017) along the European Atlantic seaboard *(Castelle et al., 2018)*. There is no significant correlation between the different climate indices (Fig. **S3d,e**).

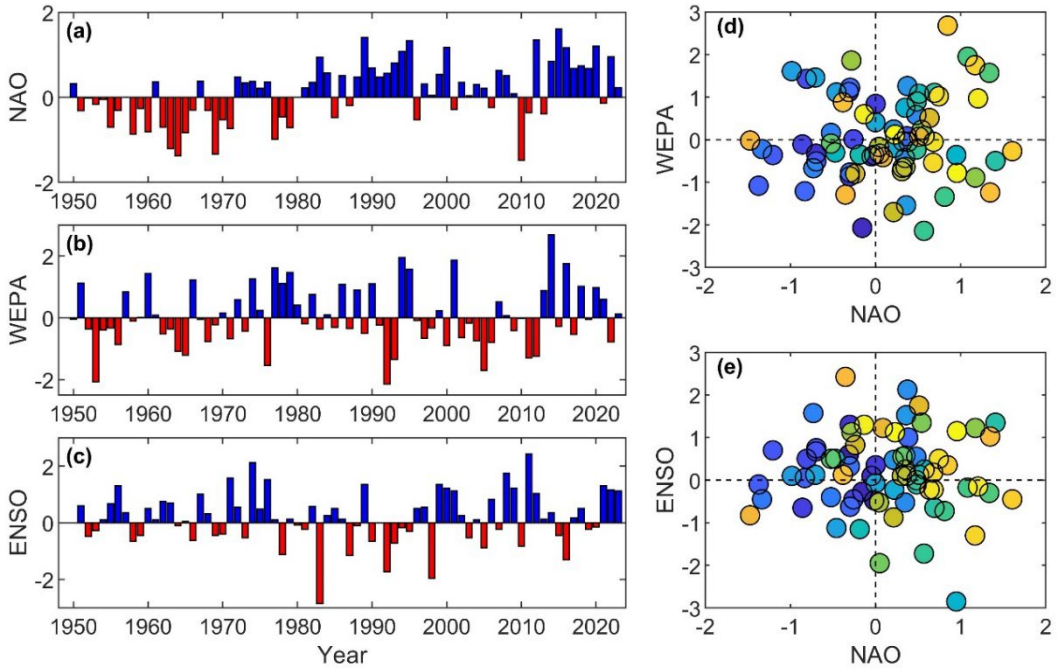

Fig. **S3**. Annual time series of: (a) North Atlantic Oscillation (NAO); (b) Western Europe Pressure Anomaly (WEPA); (c) El Nino – Southern Oscillation (ENSO); and scatter plot of (d) NAO versus WEPA, and (e) NAO versus ENSO. The color gradient associated with the symbols in the scatter plots represent 1950 (blue) to 2023 (yellow).

Both Perranporth and Slapton Sands have been surveyed monthly since 2006 by the Coastal Processes Research Group, University of Plymouth, using quad bike and walking surveys. For Perranporth, an area of 1 km x 0.5 km at the southern end of the beach is surveyed using a GPS/GNSS-mounted quad bike; on Slapton Sands several pre-defined survey lines (10–20 each month; only P01 and P18 are used here), spaced 250 m apart, are surveyed on foot using GPS/GNSS. The surveyed data represents the supra- and intertidal beach, generally down to the mean spring low tide level. The beach survey data are converted into time series of beach volume above mean low water level, nominally -2 m ODN, to a fixed backshore position that is seaward of the shortest profile, with units m^3 per unit meter of beach, thus m^3m^{-1}, or m^2. Shoreline positions, representing elevations of 0, 1, 2, 3, 4 and 5 m, are interpolated from the beach profile data. The shoreline position associated with 0 m ODN (representing c. 0.2 m above MSL) was found to best represent the beach volume (Fig. **S4a,b,c**) *(Konstantinou et al., 2023)*. The shoreline data were linearly interpolated onto a monthly time-axis which was necessary to enable extraction of the shoreline position at the start and end of winter (1 December and 1 March, respectively), and to enable computing the auto-correlation function. Directional wave buoys are installed c. 1 km off Perranporth and Slapton Sands in c. 15 and 12 m water depth, respectively, and have been recording wave conditions since 2007. These data are collected continuously at 3.84 Hz, with standard statistics reported every 30 min, and the significant wave height H_s, peak wave period T_p and the average water depth h were used to compute the 'local' wave energy flux P (i.e., without de-shoaling to obtain the deep-water wave energy flux). This paper reports on data collected over the period 2007–2023, but complete data sets for the two beaches covering the period 2007–2018, and including bathymetric and dune surveys, are reported in *McCarroll et al. (2023)*.

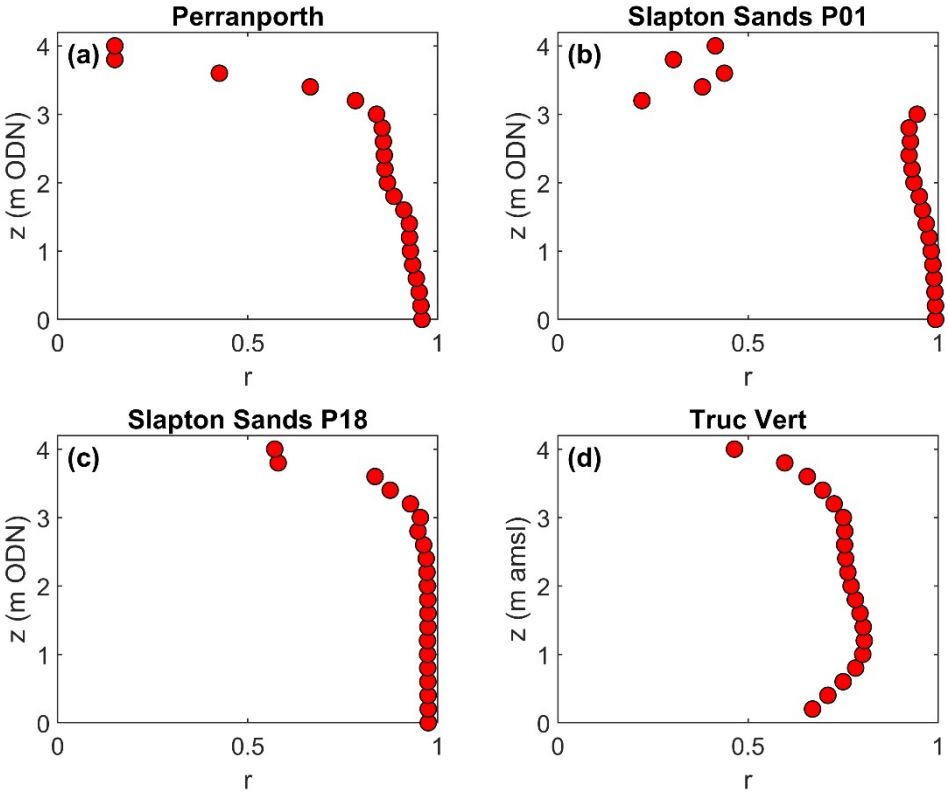

Fig. **S4**. Correlation *r* between beach volume and shoreline position defined by different contour line elevations *z* on the beach: (a) Perranporth; (b) Slapton Sands P01; (c) Slapton Sands P18; and (d) Truc Vert. For Perranporth and Slapton Sands, beach volume was computed above *z*=-2 m ODN up to a fixed backshore position, and the *z*=0 m ODN shoreline position was selected to best represent the beach volume. For Truc Vert, beach volume was computed between *z*=0 and 6 m amsl, and the *z*=1.4 m amsl shoreline position was selected to best represent the beach volume.

Truc Vert has been surveyed at monthly to bi-monthly since 2003 using walking and quad bike GPS/GNSS surveys. Surveys are performed at spring low tide, with an average transect spacing of around 50 m. The alongshore coverage progressively extended from 300 m in 2003 to over 2000 m after 2016, to both describe the alongshore-variable changes and provide robust alongshore-averaged proxies (shoreline position, volume) by smoothing out the effect of ubiquitous and prominent mega-cusp embayments. Like for Perranporth and Slapton, the surveys were converted into time series of beach volume computed between 0 m and 6 m amsl (amsl represents MSL in France) and shoreline positions were determined for different elevation proxies. Consistent with earlier work *(Robinet et al., 2016)*, the shoreline position associated with 1.4 m amsl was found to represent the beach volume best (Fig. **S4d**). The survey data collected over 2008 had issues and were removed from the analysis. As for the shoreline data from SW England, the Truc Vert shoreline data were also linearly interpolated onto a monthly time-axis. Because there are no continuous wave buoy measurements nearby Truc Vert covering the entire monitoring period, we resorted to 20 years of continuous hourly numerical wave hindcast (ERA5; *Hersbach et al., 2023*) to estimate incident wave conditions. We used the grid point closely located with the CANDHIS directional wave buoy (1° 26.8′W, 44° 39.15′N in Fig. 1a) moored in approximately 54-m depth c. 20 km SW of Truc Vert. The model wave data were compared with the measured wave data for the period July 2013 to July 2014, representing the most energetic period. Over this period, the measured and modelled H_s and P are highly correlated, with Pearson r=0.98 and 0.95, respectively. For most of the storms that occurred over the 2013/14 winter period, the ERA5 model under-predicts H_s during the storm peaks, sometimes by several meters, but the summed wave power ΣP over the 2013/14 winter period based on the ERA5 data is 96.4% of ΣP based on the measured wave data. The complete Truc Vert dataset up to 2019 is described in *Castelle et al. (2020)*.

Perranporth and Truc Vert are characterised by a unidirectional wave climate (Fig. **S2a,c**) and the shoreline response is mainly a function of the total wave power; therefore, P was summed over the months December–March to yield the total amount of winter wave power ΣP (in kWhr m^{-1}). Slapton Sands, on the other hand, is characterized by a bi-directional wave climate (Fig. **S2b**) and P was divided into a southerly and easterly component, P_{south} and P_{east}, using a directional threshold of 135°, and was summed integrated over the winter periods, yielding ΣP_{south} and ΣP_{east}. *Wiggins et al. (2019)* showed that that ΣP_{east} and ΣP_{west} should be considered collectively when attempting to understand the rotational beach response at Slapton Sands. They combined both wave power components in the annual directional power index *WDI* defined as:

$$WDI = \frac{(\sum P_{south} - \sum P_{east}) - \langle \sum P_{south} - \sum P_{east} \rangle}{\sigma(\sum P_{south} - \sum P_{east})}$$

where (ΣP_{south} - ΣP_{east}) is the difference between the southerly and easterly wave power, <ΣP_{south} - ΣP_{east}> is the long-term average of those differences (averaged over the complete survey period), and $\sigma(\Sigma P_{south} - \Sigma P_{east})$ is the standard deviation associated with the long-term average. *Wiggins et al. (2020)* further showed that the process of beach rotation, where opposing ends of the beach show anti-phase behaviour, can be quantified using a Rotation Index *RI*. To compute *RI*, the shoreline time series x for P01 and P18 were first normalized each by setting the minimum and maximum x to 0 and 1, respectively. The normalized shoreline time series x_{norm} is then used to obtain the change in the normalized volume Δx_{norm}. The beach rotation index *RI* is then computed by subtracting Δx_{norm} for P01 from that of P18. Positive values for *RI* denote clockwise rotation and negative values represent anti-clockwise rotation.

Table **S1**. Mean seasonal wave statistics* for Perranporth and Slapton Sands computed for the period 2007–2023.

	Significant wave height H_s (m)	**Peak wave period T_p (m)**	**Wave power P ($kWs^{-1}m^{-1}$)**
Perranporth - summer	1.33	9.5	13.4
Perranporth – winter	2.08	11.8	34.2
Slapton Sands – summer	0.59	7.7	2.2
Slapton Sands – winter	0.92	9.4	5.5
Truc Vert – summer	1.49	10.1	15.0
Truc Vert – winter	2.30	12.2	41.4

* Winter and summer represent December–March and April–November, respectively.

Table **S2**. Pearson correlation coefficient r and associated p-values for correlations between climate indices, and wave forcing and shoreline response. Underlined and bold *r* values are significant at the 0.05 level.

	NAO	**WEPA**	**ENSO**
Perranporth			
ΣP - $<\Sigma P>$	**0.62** (p=0.01)	**0.71** (p=0.00)	-0.23 (p=0.36)
Δx	-0.22 (p=0.40)	-0.54 (p=0.03)	0.32 (p=0.23)
Slapton Sands			
WDI	0.41 (p=0.12)	**0.68** (p=0.00)	-0.30 (p=0.26)
RI	0.09 (p=0.73)	0.47 (p=0.07)	-0.30 (p=0.25)
Truc Vert			
ΣP - $<\Sigma P>$	**0.43** (0.05)	**0.88** (0.00)	-0.09 (0.71)
Δx	-0.20 (0.42)	**-0.52** (0.02)	0.03 (0.90)

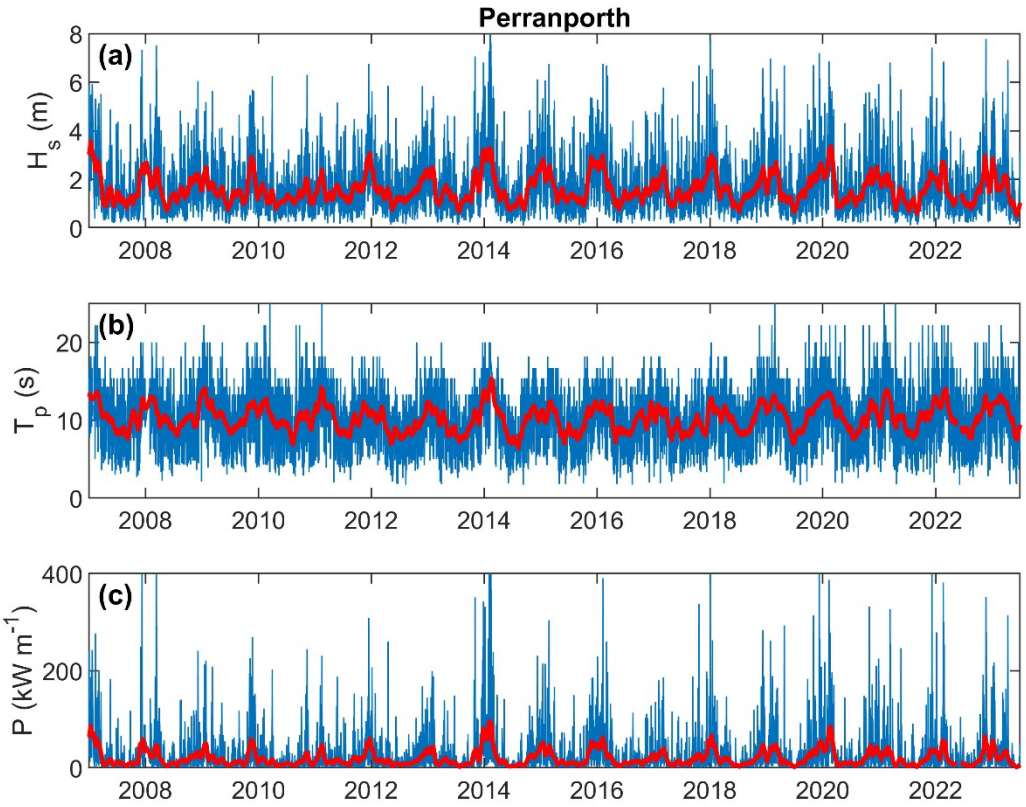

Fig. S5. Time series of wave conditions at Perranporth: (a) significant wave height H_s; (b) peak wave period T_p; and (c) wave power P for the period 2007–2023. Thick red line represents 30-day moving average.

427

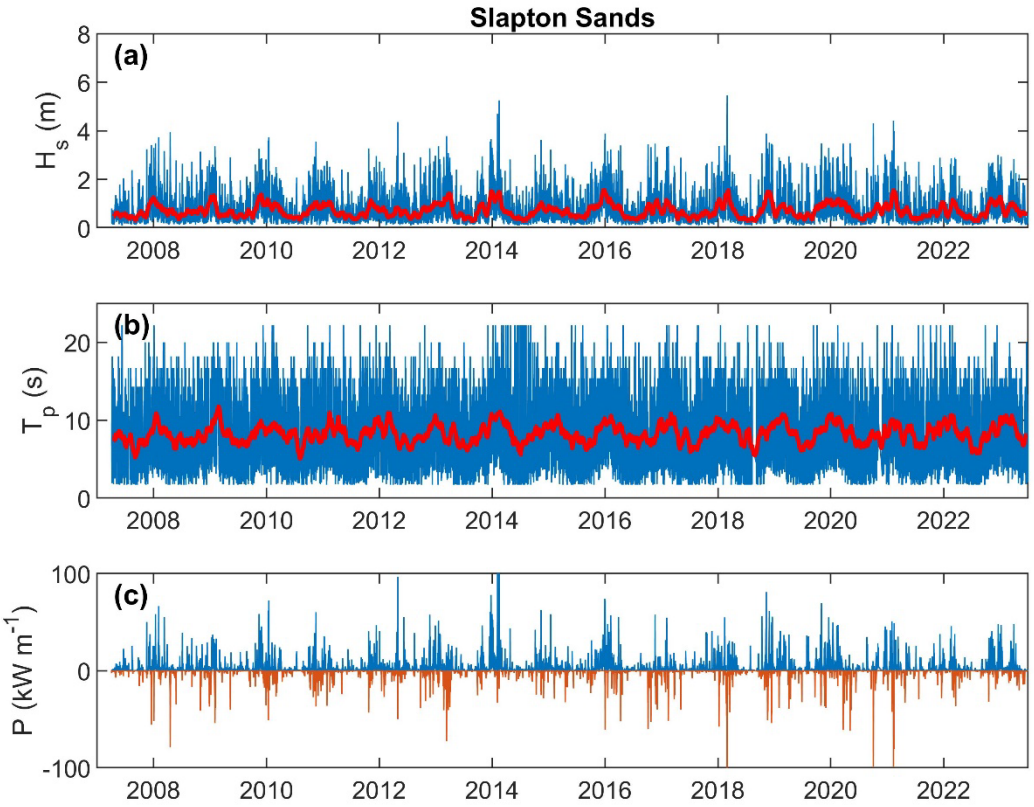

Fig. S6. Time series of wave conditions at Slapton Sands: (a) significant wave height H_s; (b) peak wave period T_p; and (c) wave power P for the period 2007–2023. Positive (blue) and negative (orange) values for P represents southerly (> 135°) and easterly waves (< 135°), respectively. Thick red line represents 30-day moving average.

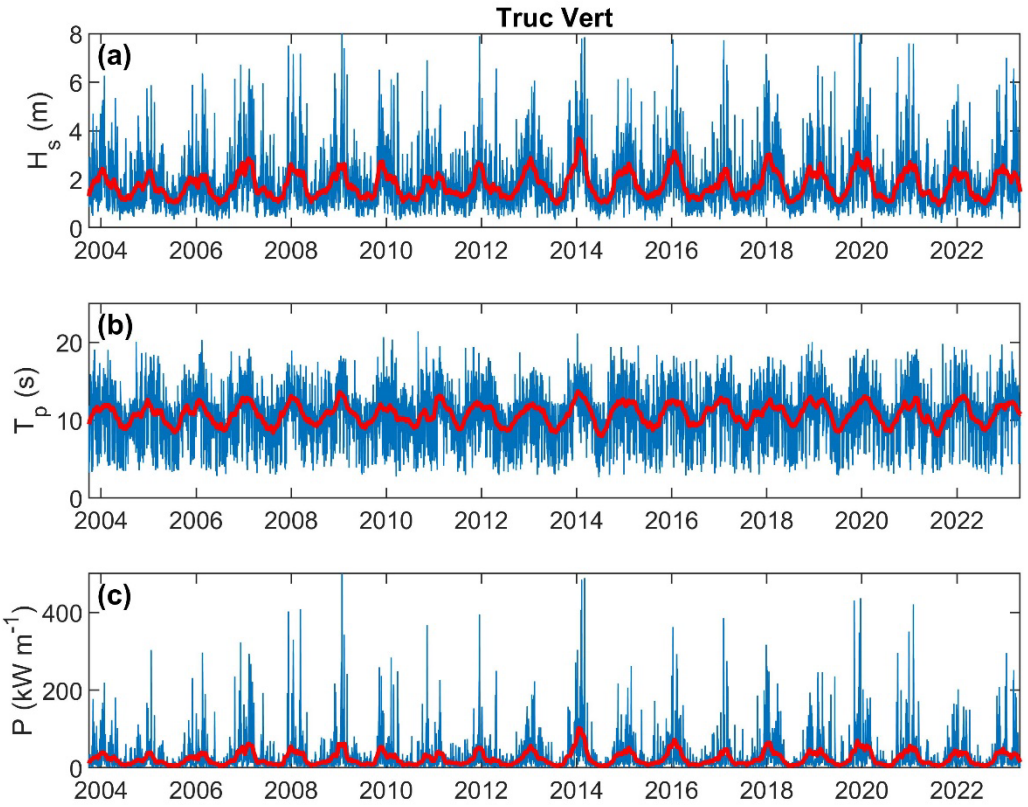

Fig. S7. Time series of modelled deep-water wave conditions at Truc Vert: (a) significant wave height H_s; (b) peak wave period T_p; and (c) wave power P for the period 2004–2023. Thick red line represents 30-day moving average.

430

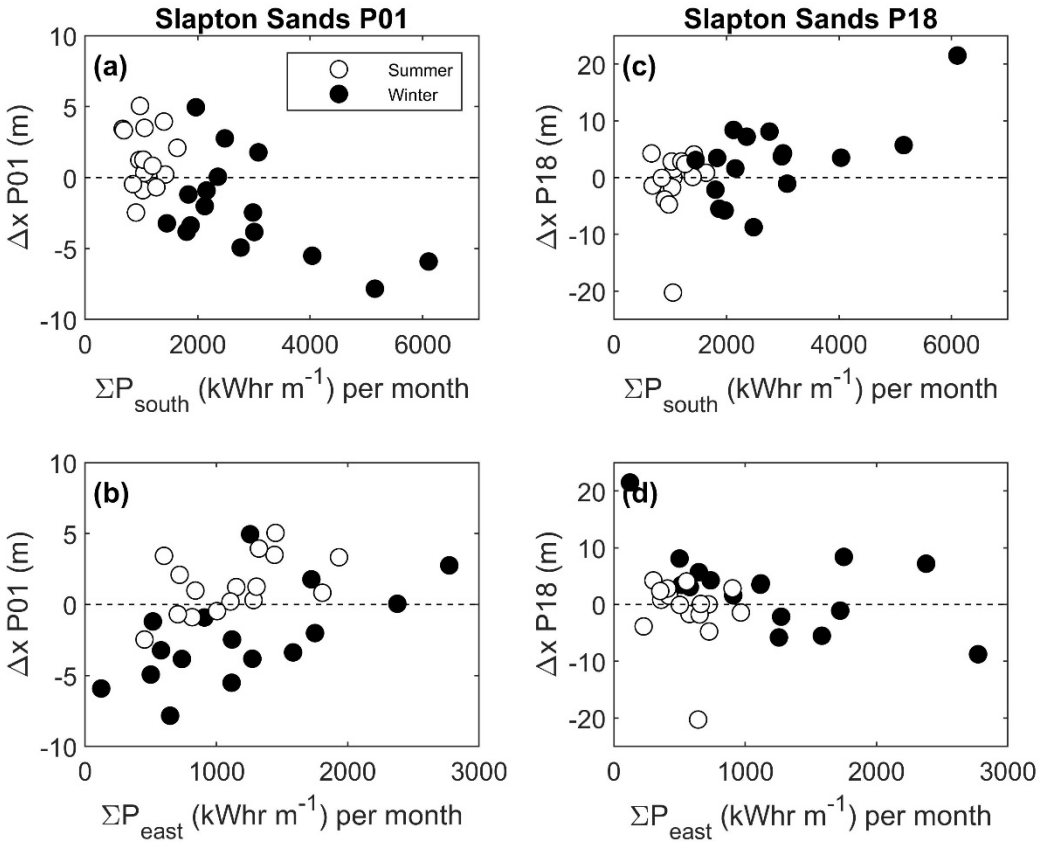

Fig. S8. Shoreline change Δx over winter (black circles) and summer (white circles) as a function of southerly and easterly wave power, ΣP_{south} and ΣP_{east}, summed over the respective seasons for profiles P01 and P18 on Slapton Sands: (a) Δx P01 versus ΣP_{south}; (b) Δx P18 versus ΣP_{south}; (c) Δx P01 versus ΣP_{east}; (d) Δx P18 versus ΣP_{east}.

431

References

ALMAR, R., BOUCHAREL, J., GRAFFIN, M., ABESSOLO, G. O., THOUMYRE, G., PAPA, F., RANASINGHE, R., MONTANO, J., BERGSMA, E. W. J., BABA, M. W. & JIN, F.-F. 2023. Influence of El Niño on the variability of global shoreline position. *Nature Communications,* 14**,** 3133.

BARNARD, P. L., ALLAN, J., HANSEN, J. E., KAMINSKY, G. M., RUGGIERO, P. & DORIA, A. 2011. The impact of the 2009–10 El Niño Modoki on U.S. West Coast beaches. *Geophysical Research Letters,* 38.

BARNARD, P. L., HOOVER, D., HUBBARD, D. M., SNYDER, A., LUDKA, B. C., ALLAN, J., KAMINSKY, G. M., RUGGIERO, P., GALLIEN, T. W., GABEL, L., MCCANDLESS, D., WEINER, H. M., COHN, N., ANDERSON, D. L. & SERAFIN, K. A. 2017. Extreme oceanographic forcing and coastal response due to the 2015–2016 El Niño. *Nature Communications,* 8**,** 14365.

BARNSTON, A. G. & LIVEZEY, R. E. 1987. Classification, Seasonality and Persistence of Low-Frequency Atmospheric Circulation Patterns. *Monthly Weather Review,* 115**,** 1083-1126.

BOUCHAREL, J., ALMAR, R., KESTENARE, E. & JIN, F.-F. 2021. On the influence of ENSO complexity on Pan-Pacific coastal wave extremes. *Proceedings of the National Academy of Sciences,* 118**,** e2115599118.

BURVINGT, O. & CASTELLE, B. 2023. Storm response and multi-annual recovery of eight coastal dunes spread along the Atlantic coast of Europe. *Geomorphology,* 435**,** 108735.

BURVINGT, O., MASSELINK, G., SCOTT, T., DAVIDSON, M. & RUSSELL, P. 2018. Climate forcing of regionally-coherent extreme storm impact and recovery on embayed beaches. *Marine Geology,* 401**,** 112-128.

CASTELLE, B., BUJAN, S., FERREIRA, S. & DODET, G. 2017a. Foredune morphological changes and beach recovery from the extreme 2013/2014 winter at a high-energy sandy coast. *Marine Geology,* 385**,** 41-55.

CASTELLE, B., BUJAN, S., MARIEU, V. & FERREIRA, S. 2020. 16 years of topographic surveys of rip-channelled high-energy meso-macrotidal sandy beach. *Scientific Data,* 7**,** 410.

CASTELLE, B., DODET, G., MASSELINK, G. & SCOTT, T. 2017b. A new climate index controlling winter wave activity along the Atlantic coast of Europe: The West Europe Pressure Anomaly. *Geophysical Research Letters,* 44**,** 1384--1392.

CASTELLE, B., DODET, G., MASSELINK, G. & SCOTT, T. 2018. Increased winter-mean wave height, variability, and periodicity in the Northeast Atlantic over 1949–2017. *Geophysical Research Letters,* 45**,** 3586-3596.

CASTELLE, B., MASSELINK, G., SCOTT, T., STOKES, C., KONSTANTINOU, A., MARIEU, V. & BUJAN, S. 2021. Satellite-derived shoreline detection at a high-energy meso-macrotidal beach. *Geomorphology,* 383**,** 107707.

CASTELLE, B., RITZ, A., MARIEU, V., NICOLAE LERMA, A. & VANDENHOVE, M. 2022. Primary drivers of multidecadal spatial and temporal patterns of shoreline change derived from optical satellite imagery. *Geomorphology,* 413**,** 108360.

COOPER, J. A. G., MASSELINK, G., COCO, G., SHORT, A. D., CASTELLE, B., ROGERS, K., ANTHONY, E., GREEN, A. N., KELLEY, J. T. & PILKEY, O. H. 2020. Sandy beaches can survive sea-level rise. *Nature Climate Change,* 10**,** 993-995.

DAVIDSON, M. 2021. Forecasting coastal evolution on time-scales of days to decades. *Coastal Engineering,* 168**,** 103928.

DISSANAYAKE, P., BROWN, J., WISSE, P. & KARUNARATHNA, H. 2015. Effects of storm clustering on beach/dune evolution. *Marine Geology,* 370**,** 63-75.

DODET, G., BERTIN, X. & TABORDA, R. 2010. Wave climate variability in the North-East Atlantic Ocean over the last six decades. *Ocean Modelling,* 31**,** 120-131.

DODET, G., CASTELLE, B., MASSELINK, G., SCOTT, T., DAVIDSON, M., FLOC'H, F., JACKSON, D. & SUANEZ, S. 2019. Beach recovery from extreme storm activity during the 2013-14 winter along the Atlantic coast of Europe. *Earth Surface Processes and Landforms,* 44**,** 393-401.

FLOR-BLANCO, G., ALCÁNTARA-CARRIÓ, J., JACKSON, D. W. T., FLOR, G. & FLORES-SORIANO, C. 2021. Coastal erosion in NW Spain: Recent patterns under extreme storm wave events. *Geomorphology,* 387**,** 107767.

GHANAVATI, M., YOUNG, I., KIREZCI, E., RANASINGHE, R., DUONG, T. M. & LUIJENDIJK, A. P. 2023. An assessment of whether long-term global changes in waves and storm surges have impacted global coastlines. *Scientific Reports,* 13**,** 11549.

HAIGH, I. D., WADEY, M. P., WAHL, T., OZSOY, O., NICHOLLS, R. J., BROWN, J. M., HORSBURGH, K. & GOULDBY, B. 2016. Spatial and temporal analysis of extreme sea level and storm surge events around the coastline of the UK. *Scientific Data,* 3**,** 160107.

HARLEY, M. D., MASSELINK, G., RUIZ DE ALEGRÍA-ARZABURU, A., VALIENTE, N. G. & SCOTT, T. 2022. Single extreme storm sequence can offset decades of shoreline retreat projected to result from sea-level rise. *Communications Earth & Environment,* 3**,** 112.

HARLEY, M. D., TURNER, I. L., KINSELA, M. A., MIDDLETON, J. H., MUMFORD, P. J., SPLINTER, K. D., PHILLIPS, M. S., SIMMONS, J. A., HANSLOW, D. J. & SHORT, A. D. 2017. Extreme coastal erosion enhanced by anomalous extratropical storm wave direction. *Scientific Reports,* 7**,** 6033.

HERSBACH, H., BELL, B., BERRISFORD, P., BIAVATI, G., HORÁNYI, A., MUÑOZ SABATER, J., NICOLAS, J., PEUBEY, C., RADU, R., ROZUM, I., SCHEPERS, D., SIMMONS, A., SOCI, C., DEE, D., THÉPAUT, J-N. 2023: ERA5 hourly data on single levels from 1940 to present. Copernicus Climate Change Service (C3S) Climate Data Store (CDS), DOI: 10.24381/cds.adbb2d47 (Accessed on 01/08/2023)

JALÓN-ROJAS, I. & CASTELLE, B. 2021. Climate Control of Multidecadal Variability in River Discharge and Precipitation in Western Europe. *Water,* 13**,** 257.

KONSTANTINOU, A., SCOTT, T., MASSELINK, G., STOKES, K., CONLEY, D. & CASTELLE, B. 2023. Satellite-based shoreline detection along high-energy macrotidal coasts and influence of beach state. *Marine Geology,* 462**,** 107082.

KONSTANTINOU, A., STOKES, C., MASSELINK, G. & SCOTT, T. 2021. The extreme 2013/14 winter storms: Regional patterns in multi-annual beach recovery. *Geomorphology,* 389**,** 107828.

KUMAR, P., KAUR, S., WELLER, E. & MIN, S.-K. 2019. Influence of Natural Climate Variability on the Extreme Ocean Surface Wave Heights Over the Indian Ocean. *Journal of Geophysical Research: Oceans,* 124**,** 6176-6199.

LUIJENDIJK, A., HAGENAARS, G., RANASINGHE, R., BAART, F., DONCHYTS, G. & AARNINKHOF, S. 2018. The state of the world's beaches. *Scientific reports,* 8**,** 1-11.

MASSELINK, G., AUSTIN, M., SCOTT, T., POATE, T. & RUSSELL, P. 2014. Role of wave forcing, storms and NAO in outer bar dynamics on a high-energy, macro-tidal beach. *Geomorphology,* 226**,** 76-93.

MASSELINK, G., BROOKS, S., POATE, T., STOKES, C. & SCOTT, T. 2022. Coastal dune dynamics in embayed settings with sea-level rise – Examples from the exposed and macrotidal north coast of SW England. *Marine Geology,* 450**,** 106853.

MASSELINK, G., CASTELLE, B., SCOTT, T., DODET, G., SUANEZ, S., JACKSON, D. & FLOC'H, F. 2016a. Extreme wave activity during 2013/2014 winter and morphological impacts along the Atlantic coast of Europe. *Geophysical Research Letters,* 43**,** 2135-2143.

MASSELINK, G. & PATTIARATCHI, C. 2001. Seasonal changes in beach morphology along the sheltered coastline of Perth, Western Australia. *Marine Geology,* 172**,** 243-263.

MASSELINK, G., SCOTT, T., POATE, T., RUSSELL, P., DAVIDSON, M. & CONLEY, D. 2016b. The extreme 2013/2014 winter storms: hydrodynamic forcing and coastal response along the southwest coast of England. *Earth Surface Processes and Landforms,* 41**,** 378-391.

MASSELINK, G., SCOTT, T., POATE, T., STOKES, C., WIGGINS, M., VALIENTE, N. & KONSTANTINOU, A. 2024. Tale of two beaches: Correlation between decadal beach dynamics and climate indices. *Coastal Sediments 2023.*

MCCARROLL, R. J., MASSELINK, G., WIGGINS, M., SCOTT, T., BILLSON, O., CONLEY, D. C. & VALIENTE, N. G. 2019. High-efficiency gravel longshore sediment transport and headland bypassing over an extreme wave event. *Earth Surface Processes and Landforms,* 44**,** 2720-2727.

MCCARROLL, R. J., VALIENTE, N. G., WIGGINS, M. H., SCOTT, T. & MASSELINK, G. 2023. Coastal survey data for Perranporth Beach and Start Bay in southwest England (2006–2021). *Scientific Data,* 10.

MENTASCHI, L., VOUSDOUKAS, M. I., PEKEL, J.-F., VOUKOUVALAS, E. & FEYEN, L. 2018. Global long-term observations of coastal erosion and accretion. *Scientific Reports,* 8**,** 12876.

MONTAÑO, J., COCO, G., CHATAIGNER, T., YATES, M., LE DANTEC, N., SUANEZ, S., CAGIGAL, L., FLOC'H, F. & TOWNEND, I. 2021. Time-Scales of a Dune-Beach System and Implications for Shoreline Modeling. *Journal of Geophysical Research: Earth Surface,* 126**,** e2021JF006169.

PLOMARITIS, T. A., BENAVENTE, J., LAIZ, I. & DEL RÍO, L. 2015. Variability in storm climate along the Gulf of Cadiz: the role of large scale atmospheric forcing and implications to coastal hazards. *Climate Dynamics,* 45**,** 2499-2514.

ROBIN, N., BILLY, J., CASTELLE, B., HESP, P., NICOLAE LERMA, A., LAPORTE-FAURET, Q., MARIEU, V., ROSEBERY, D., BUJAN, S., DESTRIBATS, B. & MICHALET, R. 2021. 150 years of foredune initiation and evolution driven by human and natural processes. *Geomorphology,* 374**,** 107516.

ROBINET, A., CASTELLE, B., IDIER, D., LE COZANNET, G., DÉQUÉ, M. & CHARLES, E. 2016. Statistical modeling of interannual shoreline change driven by North Atlantic climate variability spanning 2000–2014 in the Bay of Biscay. *Geo-Marine Letters,* 36**,** 479-490.

SCOTT, T., MASSELINK, G. & RUSSELL, P. 2011. Morphodynamic characteristics and classification of beaches in England and Wales. *Marine Geology,* 286**,** 1-20.

SCOTT, T., MCCARROLL, R. J., MASSELINK, G., CASTELLE, B., DODET, G., SAULTER, A., SCAIFE, A. A. & DUNSTONE, N. 2021. Role of Atmospheric Indices in Describing Inshore Directional Wave Climate in the United Kingdom and Ireland. *Earth's Future,* 9**,** e2020EF001625.

SPLINTER, K. D., TURNER, I. L., DAVIDSON, M. A., BARNARD, P., CASTELLE, B. & OLTMAN-SHAY, J. 2014. A generalized equilibrium model for predicting daily to interannual shoreline response. *Journal of Geophysical Research: Earth Surface,* 119**,** 1936-1958.

TONIAZZO, T. & SCAIFE, A. A. 2006. The influence of ENSO on winter North Atlantic climate. *Geophysical Research Letters,* 33.

VALIENTE, N. G., MCCARROLL, R. J., MASSELINK, G., SCOTT, T. & WIGGINS, M. 2019. Multi-annual embayment sediment dynamics involving headland bypassing and sediment exchange across the depth of closure. *Geomorphology,* 343**,** 48-64.

VITOUSEK, S., BARNARD, P. L., LIMBER, P., ERIKSON, L. & COLE, B. 2017. A model integrating longshore and cross-shore processes for predicting long-term shoreline response to climate change. *Journal of Geophysical Research: Earth Surface,* 122**,** 782-806.

VOS, K., HARLEY, M. D., TURNER, I. L. & SPLINTER, K. D. 2023. Pacific shoreline erosion and accretion patterns controlled by El Niño/Southern Oscillation. *Nature Geoscience,* 16**,** 140-146.

VOUSDOUKAS, M. I., RANASINGHE, R., MENTASCHI, L., PLOMARITIS, T. A., ATHANASIOU, P., LUIJENDIJK, A. & FEYEN, L. 2020. Sandy coastlines under threat of erosion. *Nature climate change,* 10**,** 260-263.

WARRICK, J. A., BUSCOMBE, D., VOS, K., BRYAN, K., COOPER, A., HARLEY, M., JACKSON, D., MASSELINK, G., PALMSTEN, M., RUIZ DE ALEGRIA-ARZABURU, A., SÉNÉCHAL, N., SHERWOOD, C., SHORT, A., SOGUT, E., SPLINTER, K., STEPHENSON, W., SYVITSKI, J., WOODROFFE, C., YOUNG, A. 2024. Evaluating climate signals on global shoreline positions – A commentary on “Influence of El Niño on the variability of global shoreline position” by Almar et al. *Nature Communications*.

WARRICK, J. A., VOS, K., BUSCOMBE, D., RITCHIE, A. C. & CURTIS, J. A. 2023. A Large Sediment Accretion Wave Along a Northern California Littoral Cell. *Journal of Geophysical Research: Earth Surface,* 128**,** e2023JF007135.

583 WIGGINS, M., SCOTT, T., MASSELINK, G., MCCARROLL, R. J. & RUSSELL, P. 2020. Predicting beach
584 rotation using multiple atmospheric indices. *Marine Geology***,** 106207.
585 WIGGINS, M., SCOTT, T., MASSELINK, G., RUSSELL, P., CASTELLE, B. & DODET, G. The role of multi-
586 decadal climate variability in controlling coastal dynamics: re-interpretation of the 'lost
587 village of Hallsands'. 2017 2017. 96-107.
588 WIGGINS, M., SCOTT, T., MASSELINK, G., RUSSELL, P. & MCCARROLL, R. J. 2019. Coastal embayment
589 rotation: Response to extreme events and climate control, using full embayment surveys.
590 *Geomorphology,* 327**,** 385-403.
591 YATES, M. L., GUZA, R. T. & O'REILLY, W. C. 2009. Equilibrium shoreline response: Observations and
592 modeling. *Journal of Geophysical Research: Oceans,* 114.
593 YOUNG, A. P., FLICK, R. E., GALLIEN, T. W., GIDDINGS, S. N., GUZA, R. T., HARVEY, M., LENAIN, L.,
594 LUDKA, B. C., MELVILLE, W. K. & O'REILLY, W. C. 2018. Southern California Coastal Response
595 to the 2015–2016 El Niño. *Journal of Geophysical Research: Earth Surface,* 123**,** 3069-3083.
596 ZĂINESCU, F., ANTHONY, E., VESPREMEANU-STROE, A., BESSET, M. & TĂTUI, F. 2023. Concerns about
597 data linking delta land gain to human action. *Nature,* 614**,** E20-E25.

598